Variation of skyrmion forms and their stability in MnSi thin plates

Xiuzhen Yu,[1] Akiko Kikkawa,[1] Daisuke Morikawa,[1] Kiyou Shibata,[2] Yusuke Tokunaga,[1]
Yasujiro Taguchi,[1] and Yoshinori Tokura[1,2]
[1]*RIKEN Center of Emergent Matter Science (CEMS), Wako 351-0198, Japan*
[2]*Department of Applied Physics and Quantum Phase Electronics Center (QPEC), University of Tokyo, Tokyo 113-8656, Japan*
(Received 3 December 2014; revised manuscript received 22 January 2015; published 17 February 2015)

By systematic real-space observations using Lorentz transmission electron microscopy, we report here various forms of skyrmions (and related spin textures) for a prototype of cubic helimagnet MnSi as well as their stability that depends on crystalline-orientation and crystal-plate thickness. Below a crossover thickness ($t_c \sim 75$ nm) of a sample, the robust two-dimensional hexagonal skyrmion crystal (SkX) appears over a wide window of temperature and magnetic field, regardless of crystal orientation, while the SkX phase region shrinks to a small pocket near the helical transition temperature T_N in a (111) plate with the thickness above t_c, in contrast to the stable SkX in (110) and (001) plates. This observation indicates the importance of the magnetic anisotropy and thermal fluctuation effects for the skyrmion stability. Furthermore, the forms of skyrmions have been found to change from multidomain state of SkX to skyrmion glass structure via single domain state of SkX with increasing magnetic field.

DOI: 10.1103/PhysRevB.91.054411 PACS number(s): 12.39.Dc, 64.60.an, 75.60.Lr, 03.75.Lm

I. INTRODUCTION

A skyrmion is a topological particlelike object whose concept was originally introduced in field theory of nucleons [1]. A magnetic skyrmion is a vortexlike topological spin texture emerging in magnetic materials [2]. Skyrmions have the potential for application in spintronics owing to their emergent electromagnetic phenomena, such as topological Hall effect (THE), skyrmion Hall effect [3] [a Hall motion of the skyrmion crystal (SkX) itself as the counteraction of the THE], and the ultralow current driven skyrmion motion [3–15]. In order to develop technologies which manipulate skyrmions, it is important to understand first the variation of skyrmion forms and their stability.

The skyrmion lattice phase, called A phase [4], was directly observed first by a small-angle neutron scattering (SANS) study for a helimagnet MnSi, which has a cubic chiral crystal structure and a helical magnetic structure with periodicity of ~19 nm [4] induced by a Dzyaloshinskii-Moriya interaction (DMI) [16]. In the A phase, a skyrmion lattice with sixfold symmetric SANS spots was observed in the plane perpendicular to the external magnetic fields irrespective of the crystalline-orientation, although the helical axis tends to align along the [111] axis [4]. In bulk MnSi, the A phase appears in a relatively narrow window of temperature (T) and the magnetic field (B) near the helical transition temperature (T_N). The A phase appears to be most unstable for $B//[111]$ [17].

As for the epitaxial thin films, a recent paper [18] stressed the role of strain-induced uniaxial anisotropy in determining the magnetic texture in (111) epitaxial MnSi thin film; it was argued that, in contrast to the A phase (SkX) that appears around T_N in bulk MnSi, only conical structure forms with an application of perpendicular magnetic field for (111) thin film due to the out-of-plane hard axis. Such magnetic anisotropy tends to suppress the in-plane helical propagation vector and instead favors the out-of-plane helical or cone modulation structure. On the other hand, it was claimed that formation of skyrmions was observed by measurements of Lorentz transmission electron microscopy (LTEM) as well as THE in (111) epitaxial thin film of MnSi [19]. Therefore, the effect of anisotropy on the formation of skyrmion remains elusive.

Another important parameter to determine the skyrmion stability is the spatial dimensionality. For example, skyrmion phase or SkX is conspicuously stabilized for thin plate forms of $B20$-type helimagnets $Fe_{0.5}Co_{0.5}Si$ and FeGe, in particular with film thickness (<50 nm) below the helical period [meaning magnetically two-dimensional (2D) films] [5,20]; the thinner plate sample has a much wider window of SkX phase in the T–B plane compared with the bulk case [5,20]. Qualitatively, this is because the conical structure is lower in energy under magnetic field in the usual three-dimensional (3D) bulk cases; however, the conical state with the modulation normal to the film plane shows less energy gain in 2D thin films due to the incomplete helix formation or the effect of helix cutoff at the top/bottom surfaces [5]. It is also theoretically argued that skyrmion (in-plane helix) is stable under (without) vertical magnetic field as compared with the conical state as the film thickness becomes very thin [21]. Although the SkX is generally more stable in 2D than in 3D systems, there have been so far no clear experimental results systematically characterizing the thickness dependence of skyrmions in MnSi by means of real-space observation, due partly to its low magnetic-transition temperature (below 30 K) and partly to the minuscule size (approximately 22 nm in diameter) close to the spatial resolution of real-space observation. The field-dependent evolution of skyrmion-related spin textures is also still unclear. MnSi is the most prototypical material to host the skyrmion as well as the other helical spin textures. In this context, the LTEM study is expected to provide the solutions to the following basic questions: (1) Can skyrmions be realized in (111) MnSi thin samples under an external magnetic field, which is parallel to the hard axis? (2) What is the relationship between the crystalline orientation and the skyrmion stability? (3) How does the spin texture evolve from the helical structure via various forms of skyrmion to the induced ferromagnetic state with increasing a magnetic field?

 ©2015 American Physical Society

To tackle these questions, we have prepared (111), (110), and (001) single-crystalline thin plates of MnSi with thickness gradients and systematically investigated the relationship among the crystalline orientation, sample thickness, and skyrmion stability as well as the field evolution of the skyrmionic spin texture by means of the LTEM. The thickness dependence of SkX shows that below a crossover thickness t_c($\sim$75 nm), regardless of the crystalline orientation, in-plane helical modulation vectors appear in zero field, and SkX shows up in a wide range of T and B. Above the t_c for (111) plate, the in-plane helical vector in zero field disappears, yet SkX shows up upon application of normal magnetic field at higher temperatures near T_N, while (110) and (001) plates show in-plane helical vectors in zero field as well as SkX upon application of magnetic field. These observations indicate that dipolar interaction and thermal fluctuation stabilize SkX. Furthermore, the forms of skyrmions have been found to change from the multidomain state of SkX to skyrmion glass (SkG) structure via single domain state of SkX with increasing magnetic field.

II. EXPERIMENTAL

A single crystal of $B20$-type MnSi was grown by Czochralski method with a tetra-arc furnace. A mixture of Mn and Si with an atomic ratio of 1:1 was arc melted in an argon atmosphere, and then single-crystal MnSi was pulled with use of a seed crystal. The powder x-ray diffraction confirmed that the as-grown crystal is of the single phase of $B20$-type cubic structure. The orientation of the MnSi crystal was determined by Laue diffraction, and then thin plates were cut from the bulk sample and then further thinned by mechanical polishing and argon ion milling (Gatan PIPS was operated at 4 kV). The crystalline orientation of the thin plates was also checked by selected-area electron diffraction (SAED). The thickness map of the thin plates was obtained by electron energy-loss spectroscopy (EELS). Note here that EELS measurements only provide the ratio of thickness to mean free path length [22], which must be measured or calculated by an independent method. By combining convergent beam electron diffraction (CBED) measurements, the error of sample thickness measured by EELS becomes less than 10%.

Magnetic domain structures were studied by LTEM observations, which have been carried out at a low magnification mode of a high-throughput transmission electron microscope (JEM-2800) with a thermal-field-emission electron gun at an acceleration voltage of 200 kV. A liquid-helium-cooled sample holder (Gatan ULTDT) was used to study the temperature dependence of the magnetic textures. By using LTEM, the in-plane magnetizations can be imaged as convergence (bright contrast) or divergence (dark contrast) of the electron beam on the defocused (under- or overfocused) image planes. The inversion of such magnetic contrast can be seen between the over- and underfocused images [10]. The defocus distance was calibrated as a function of the objective minilens current. To observe the spontaneous helical structures of MnSi thin plates at zero magnetic field, we switched off the magnetic-objective lens current of the electron microscope and obtained the LTEM images. To induce magnetic skyrmions, we gradually increased the objective lens current to increase the magnetic field, which was applied perpendicularly to the MnSi thin plate plane. The magnitude of the magnetic field at the sample position was measured in advance by a Hall probe as a function of the objective lens current.

To obtain quantitative information on the in-plane magnetizations, we analyzed the LTEM images by using a software package QPt (HREM Co.), which is based on the transport-of-intensity equation (TIE) [23]. The analysis allowed us to obtain the local magnetization textures for the MnSi thin plates.

III. RESULTS AND DISCUSSION

A. Spin textures depending on crystalline orientation of the MnSi thin plate

The LTEM observations for single-crystalline samples unambiguously demonstrated that robust hexagonal SkX can form in all the (111), (110), and (001) thin plates with a thickness of 30 nm by applying a magnetic field normal to the plates. Figures 1(a)–1(c) show zero-field magnetic stripe (proper screw spins) domains at 6 K in (a) (111), (b) (110), and (c) (001) plates. Single stripe domain, two domains of stripes (A domain and B domain) with small-angle grain boundaries, and twin of stripe domains (C domain and D domain) with periodicity of approximately 18 nm were clearly discerned for (111), (110), and (001) plates, respectively. Analysis of SAED (shown as the upper insets) and fast Fourier transforms (FFT) of LTEM images (shown as the lower insets) indicates that the in-plane propagation vectors of helices were along the [11-2] axis, the ⟨111⟩ axes and the ⟨110⟩ axes in (111), and the (110) and (001) MnSi thin plates, respectively, while the spontaneous helical vector tends to lie along ⟨111⟩ axes in the MnSi bulk sample due to magnetocrystalline anisotropy. It means that the helices are flexible to some extent and that the in-plane propagation vectors show up in the thin plate samples as the thickness becomes comparable to the helical period. The direction of helical modulation in thin plates is determined by the competition between the magnetic anisotropic energy gain with spins lying perpendicular to ⟨111⟩ and the loss of DMI energy due to the incomplete helix formation along the normal direction. The observed in-plane helical modulation indicates that the latter interaction becomes dominant to switch the out-of-plane helix to the in-plane one in such a thin (111) MnSi plate with thickness of 30 nm. When the external magnetic field was applied perpendicular to the in-plane helices, the magnetic skyrmion should be induced.

Figures 1(d)–1(f) show magnetic SkX structures for (d) (111), (e) (110), and (f) (001) thin plates (30 nm thick) of MnSi under the magnetic fields applied perpendicular to the plates. The FFTs shown as the insets clearly indicate hexagonal symmetry for the SkX. Interestingly, the single domain of SkX emerges under the appropriate magnetic fields in spite of the presence of twin domains of helical structure or small-angle grain boundaries at zero magnetic field. We have also examined the skyrmion helicity for all of the MnSi thin plates. By analyzing a pair of the LTEM images (underfocused and overfocused images) with the TIE, we have obtained the magnetization maps of SkX, which are presented in Figs. 1(g)–1(i) for the cell

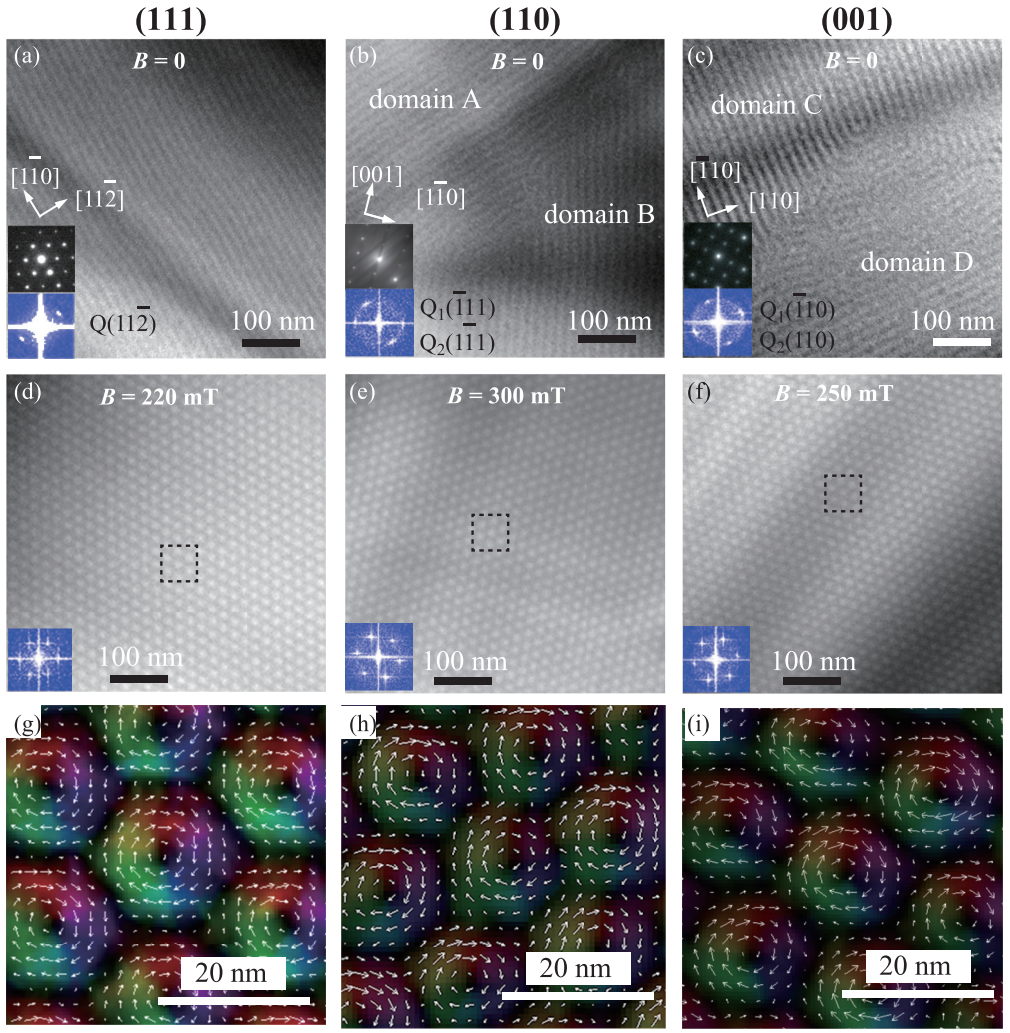

FIG. 1. (Color online) (a)–(f) LTEM images (defocus distance $\sim -30\,\mu$m) at 6 K [(a)–(c) in zero field and (d)–(f) in a magnetic field] and (g)–(i) magnetization maps for one unit cell of SkX as derived from TIE analysis of the data shown within dashed squares in (d)–(f). (a), (d), (g); (b), (e), (h); and (c), (f), (i) are for (111), (110), and (001) thin plates, respectively. The thickness of these thin plates is around 30 nm. Insets at the lower left corners of (a)–(f) are SAED patterns (upper) and FFT (lower) of LTEM images. Colors and white arrows in (g)–(i) indicate the magnitude and direction of in-plane magnetizations, while the black area shows zero in-plane magnetization or out-of-plane magnetization. (a)–(c) Helimagnetic stripe domain structures at zero magnetic field; (d)–(f) magnetic SkX with hexagonal symmetry under normal magnetic fields of 220 mT, 300 mT, and 250 mT, respectively. All LTEM images were taken at the underfocused Lorentz mode.

of SkX in the (111), (110), and (001) MnSi thin plates. Such characterization of magnetizations in SkX proved the unique magnetic helicity of the skyrmions in single-crystalline MnSi plates.

Compared to magnetic textures observed in the epitaxial MnSi thin film [19], two major differences have been observed here for the free-standing thin plate specimens. One is that the periodicity ($\sim$18 nm) of the helical structure without a magnetic field is close to the value [4] (=19 nm) reported for bulk samples, while that of the epitaxial thin film is rather reduced to 8.5 nm [19]. The other is that the almost perfect hexagonal skyrmion lattice is stabilized in the present thin plate under magnetic fields, whereas that of the epitaxial film is highly disordered. These differences are probably due to the fact that the free-standing plate specimens thinned down from a bulk single crystal are free from the lattice strain and also from the crystalline-chirality disorder (chirality-domain distribution) that are present in the epitaxial thin film.

B. Variation of skyrmion forms with changing external magnetic field

The field dependence of the LTEM images [Figs. 2(a)–2(f)] and their FFTs (the respective insets) at 18 K for a (111) MnSi thin plate represent a variety of magnetic textures. The helical modulation propagates along the [11-2] axis in the zero magnetic field [Fig. 2(a)] but begins to curl around the randomly distributed singularity points with a weak normal field [Fig. 2(b)]. The ring FFT pattern (the inset at the right upper corner) of the real-space LTEM image clearly demonstrates that the reflections related to helical propagation vectors rotate in the plane. Hereafter, this state will be referred to as the random/rotating-q helix (Rq-H) state. With the increase in magnetic field, a multidomain state of hexagonal

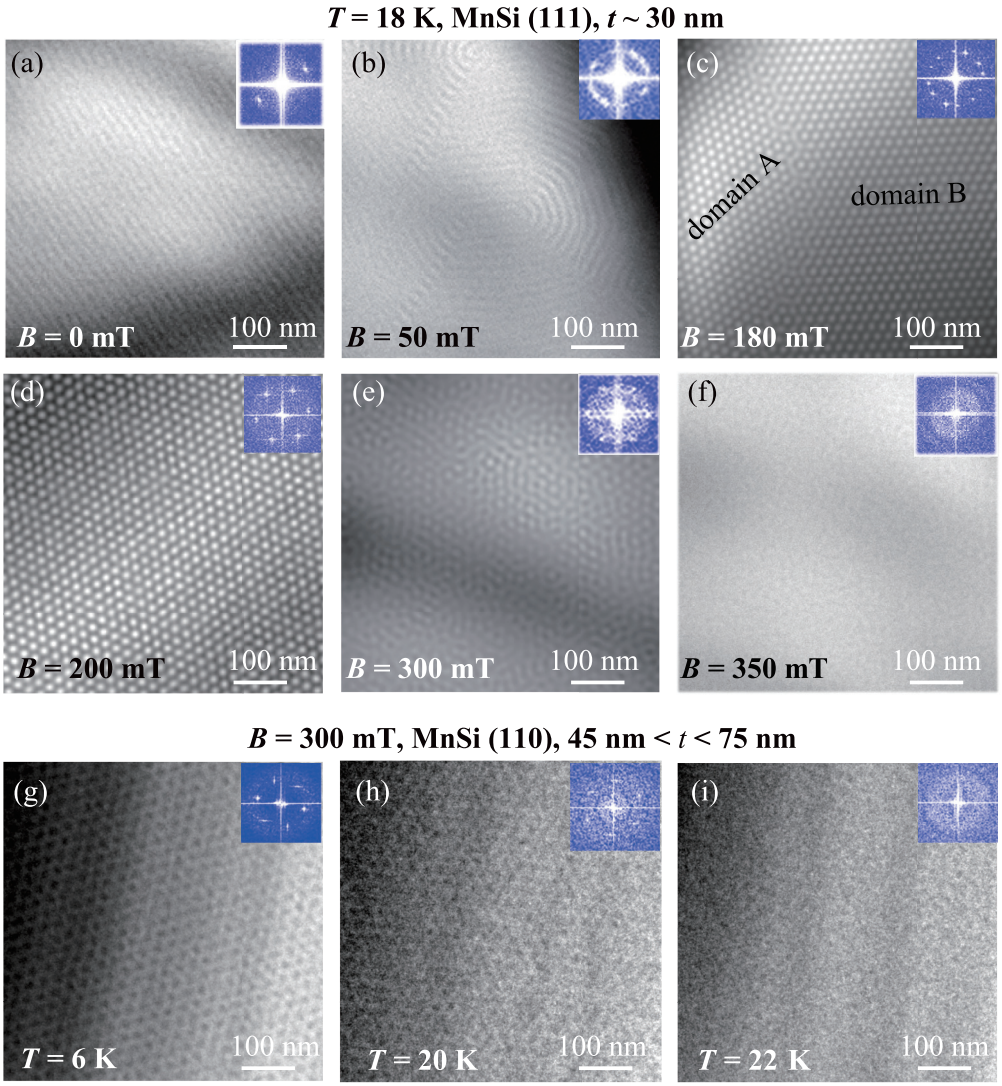

FIG. 2. (Color online) (a)–(f) Changes in magnetic textures in a (111) thin plate with the thickness of ~30 nm with varying magnetic fields at 18 K. LTEM images (underfocus, defocus distance $\sim -36\,\mu$m) and corresponding FFTs (insets) obtained under various magnetic fields demonstrate (a) the helical structure with an in-plane propagation vector in zero magnetic field, (b) random/rotating-q stripes under a weak field of 25 mT, (c) two domains of SkX, (d) single-domain state of SkX, (e) SkG structure with an obscured FFT pattern, and (f) single-domain state of field-induced ferromagnetic structure. (g)–(i) Temperature evolution of skyrmion form observed at the overfocused Lorentz mode (defocus distance $\sim 36\,\mu$m) for a (110) plate with the thickness of 45 nm $< t <$ 75 nm at a constant field of $B = 300$ mT from (g) single SkX to (i) paramagnetic structure via (h) SkG. Insets show the corresponding FFT of LTEM images.

SkX appears, as shown in Fig. 2(c); two sets of sixfold reflections related to two domains (referred to as domain A and B) are clearly observed in the FFT. Further increase of external field drives the multidomain state to a perfect single domain state of SkX [Fig. 2(d)], while under a higher field the single-domain SkX is destabilized and changes to SkG structure, as characterized by an obscured FFT pattern [Fig. 2(e)]. Finally, a single domain with the magnetization normal to the plate plane is formed as observed as the no-contrast LTEM picture [Fig. 2(f)]. The SkG structure has been also observed with heating the (110) thin plate from 6 K up to 22 K under a constant field of 300 mT, as shown in Figs. 2(g)–2(i); the temperature dependence of SkX forms and their FFTs (insets) represents a variety of magnetic textures from a single domain structure of (g) hexagonal SkX to (i) paramagnetic state via (h) SkG.

C. Crossover thickness for skyrmion lattice formation in a (111) MnSi thin plate

Next, we investigate the plate thickness effect on SkX formation. Figures 3(a), 3(b) represent the thickness map and its averaged line profile for a (111) MnSi plate with thickness gradient, as obtained by EELS [23,24]. The important thickness effect on spiral structure (stripe) originally showing the "easy" modulation vector along the [111] was revealed by a real-space LTEM image shown in Fig. 3(c); the in-plane helical structure is stabilized in zero field in the thinner regions with the thickness below $t_c \sim 75$ nm, while it disappears in the thicker region than t_c, suggesting the probable out-of-plane helical modulation of spin spiral structure. The FFT of LTEM images at 6 K without a magnetic field [Figs. 3(d)–3(g)] and those under a magnetic field of 290 mT [Figs. 3(h)–3(k)] also systematically demonstrate that neither spontaneous in-plane

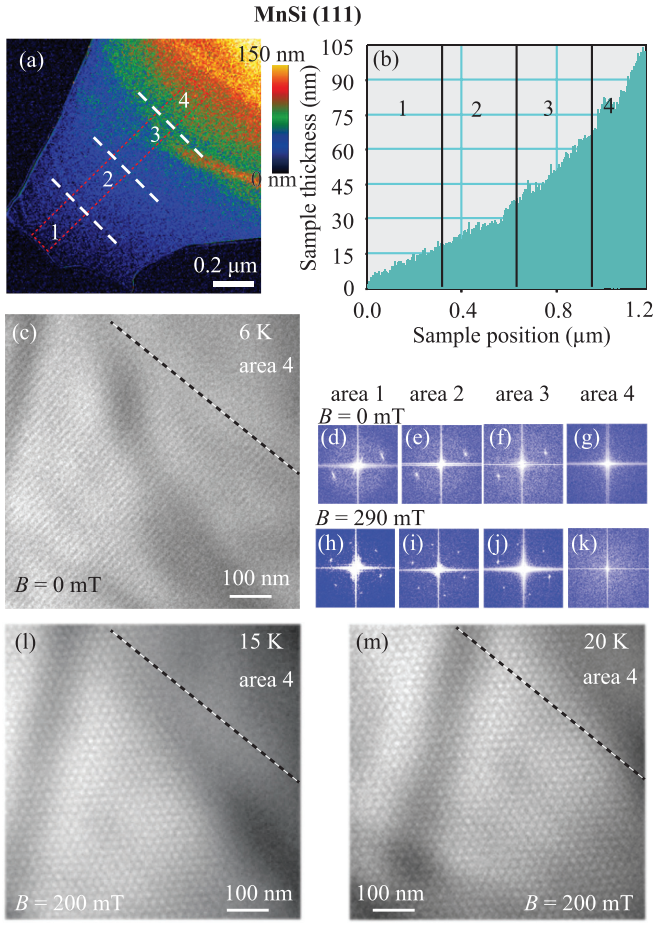

FIG. 3. (Color online) Thickness dependence of magnetic structures in a wedge-shaped (111) MnSi plate. (a), (b) 2D thickness map obtained by EELS and the averaged line profile [over the surrounded area with red dashed lines shown in (a)] of the sample thickness, respectively. (c) LTEM image taken under zero field at 6 K. The defocus distance is approximately $-30\,\mu$m. Dashed line indicates the boundary between areas 3 and 4. (d)–(g) FFT of each local LTEM image for areas 1–4 taken at 6 K under zero magnetic field and (h)–(k) under 290 mT field. (l), (m) LTEM images for the same area as presented in (c), obtained under 200 mT field at (l) 15 K and (m) 20 K, respectively.

spiral structure nor hexagonal SkX under magnetic field appears in the thicker region (area 4) at this low temperature, in contrast to the robust in-plane stripes and field-induced SkX in the thinner regions (areas 1–3) of the plate. This indicates that the magnetic anisotropy dominates and induces a favorable out-of-plane modulated screw and conical structure, respectively, without field and under normal magnetic field, when the sample is thick enough. The reduction of the sample thickness is likely to enhance the loss in the DMI energy gain for the case of incomplete helix formation along the normal ([111]) direction. When the thickness is below a crossover thickness (t_c), the modulation vector slants away from out of plane to in plane.

Interestingly, the temperature dependence of the LTEM images under the 200 mT field shown in Figs. 3(l) and 3(m) reveals that the hexagonal SkX emerges even in area 4 with the increase in sample temperature near T_N; when we increase the temperature up to 20 K, the hexagonal SkX emerges and extends over area 4 under a perpendicular field of 200 mT despite the absence of an in-plane helical vector at zero magnetic field in the same area 4. Thus, to understand the skyrmion stability in $B20$-type system, the thermal fluctuation effect should be taken into account also in the thin film case. Another point to be noted here is that the magnetic contrast was observed for a very thin area (even 10 nm thickness in area 1), as clearly exemplified by the FFTs of helical and SkX structures [Figs. 3(d), 3(h)], in contrast to a recent prediction [24] that the minimum thickness for the observation of skyrmions is 17 nm for MnSi.

D. Skyrmion phase diagrams depending on crystalline orientation and thickness of MnSi thin plate

Based on the systematic LTEM observations for three MnSi thin plates with different orientations [(111), (110), and (001)] and thickness gradient, we established magnetic phase diagrams, as shown in Fig. 4. The thickness maps obtained by EELS measurements shown in Figs. 4(a)–4(c) indicate that the sample thickness changes from 0 to above 120 nm for all of the wedge-shaped (111), (110), and (001) plates. The LTEM measurements for such wedge-shaped thin plates allowed us to obtain the thickness dependence of the magnetic phase diagram. In the thicker regions of the MnSi plates with the thickness (75 nm to 120 nm) above $t_c \sim 75$ nm, clear differences of the SkX phase are observed for the (111) plate versus the (110) and (001) plates. In the thicker (111) plate with $t > t_c$, the SkX phase shrinks to a small pocket [Fig. 4(d)], almost approaching the A phase region in MnSi bulk [25] in the T-B plane, while the robust SkX phase prevails in a wide window of the T-B plane in (110) and (001) plates [Figs. 4(e), 4(f)]. Another difference is that the helical propagation vector in zero field lies within the plane for (110) and (001), while the vertical helical structure with the modulation vector normal to the (111) plate is the most plausible one for (111) plate. As the sample thickness becomes less than the crossover thickness $t_c \sim 75$ nm [Figs. 4(g)–4(l)], regardless of the crystal orientation, the SkX phase subsists down to 6 K. These phase diagrams indicate that the thick (111) plate is rather unique among the samples investigated, where the vertical spiral structure is favored in the absence of magnetic field and the vertical conical structure shows up upon application of the field at low temperatures. More unexpectedly, contrary to the relatively stable SkX in (111) and (001) plates, SkX changes to the SkG structure [shown in Fig. 2(h)] near T_N in the (110) thin plate, while the most favorable helical propagation vector (i.e., $\langle 111 \rangle$) is within the plane in this orientation. The reason for the disappearance of the helical stripe in (110) thin plate at lower temperatures, which was also observed in the previous study [26], is not clear at the current stage.

IV. CONCLUSION

In conclusion, systematic real-space LTEM observations unveil the crystalline-plane and plate-thickness dependences of skyrmion forms and their stability in $B20$-type cubic helimagnet MnSi: Such a variation is mostly attributed to the competition between the weak uniaxial magnetic anisotropy and the DMI energy in the finite-thickness plate. Based on

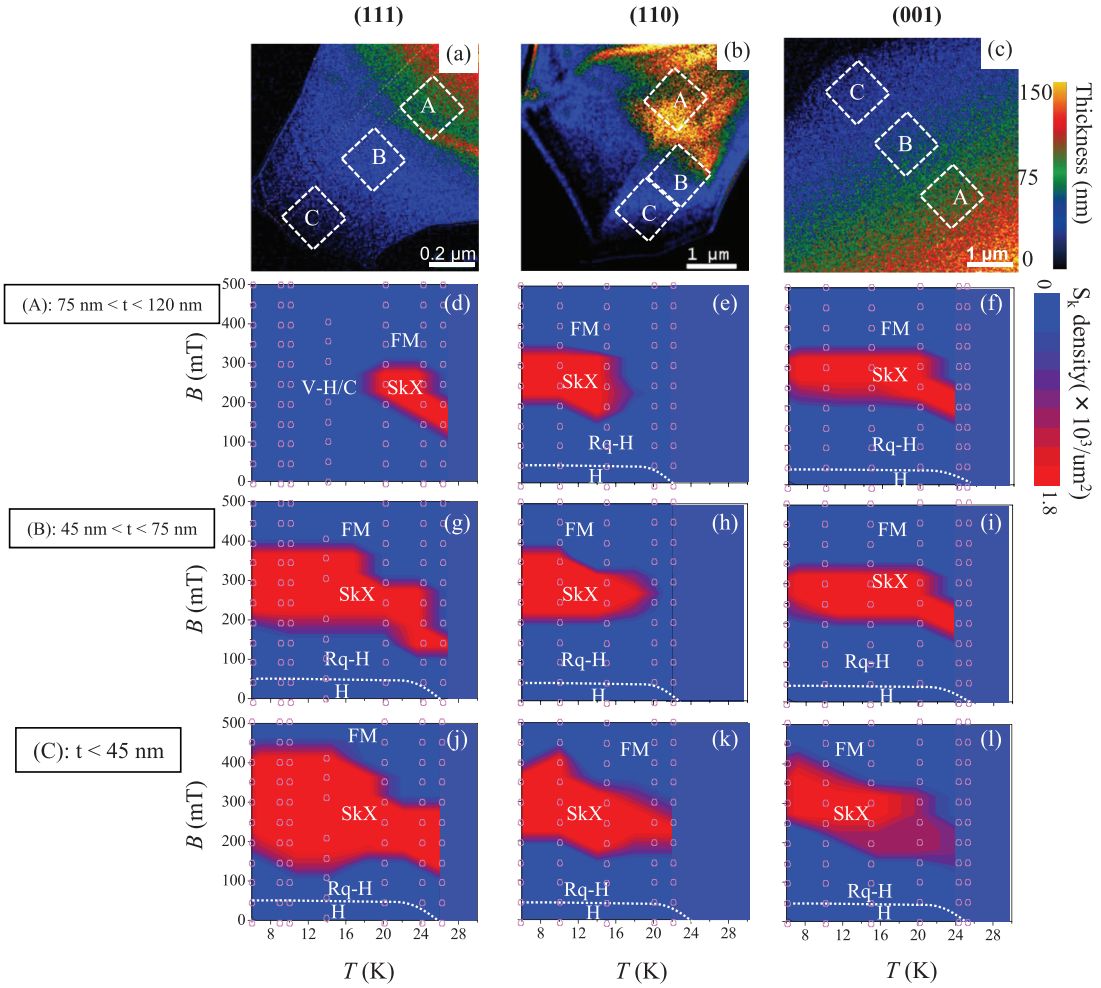

FIG. 4. (Color online) Magnetic phase diagrams obtained for wedge-shaped (111), (110), and (001) MnSi thin plates with thickness gradient. (a)–(c) 2D thickness maps of the (a) (111), (b) (110), and (c) (001) plates, respectively. The phase diagrams in the *T*-*B* plane obtained in (A) thick regions with thickness of 75 nm $< t <$ 120 nm [(d)–(f)], (B) intermediate-thickness regions between 45 nm and 75 nm [(g)–(i)], and (C) thin regions with thickness below 45 nm [(j)–(l)]. These diagrams are obtained from LTEM images taken at the regions designated as A, B, and C, respectively, in (a)–(c). H, Rq-H, SkX, V-H/C, and FM are the in-plane helical structure, random/rotating-q helical structure, skyrmion crystal state, (possibly) vertical helical or conical structure, and field-induced ferromagnetic state, respectively. The open circles show the data points where LTEM snapshots were taken.

extensive LTEM observations, we have concluded that (1) the robust hexagonal SkX phase exists in a wide window of the *T*-*B* plane and shows minimal dependence on crystalline orientation in thin MnSi plate with sample thickness below t_c(∼75 nm); (2) in contrast to the robust SkX in (110) and (001) MnSi, the in-plane spiral structure in zero field disappears and the SkX phase window shrinks in the *T*-*B* plane for thicker (111) MnSi with thickness above t_c. This observation indicates a favorable vertical spiral structure at the ground state and possible conical structure under normal magnetic fields due to the dominant effect of magnetic anisotropy in the (111) plate with increasing thickness; (3) increasing magnetic field can drive the crystallographic form of skyrmion from multidomain state of SkX to the single-crystalline state of SkX and further to the skyrmion glass structure in the (111) MnSi thin plate.

ACKNOWLEDGMENTS

We gratefully thank N. Nagaosa and T. Arima for enlightening discussions. This paper was in part supported by the Funding Program for World-Leading Innovative R&D on Science and Technology (FIRST program) on "Quantum Science on Strong Correlation." This paper was also supported in part by the Japan Society for the Promotion of Science (JSPS) Grant-in-Aid for Scientific Research(S) No. 24224009.

[1] T. Skyrme, Nucl. Phys. **31**, 556 (1962).
[2] A. N. Bogdanov and D. A. Yablonskiĭ, Zh. Eksp. Teor. Fiz. **95**, 178 (1989).
[3] N. Nagaosa and Y. Tokura, Nat. Nanotech. **8**, 899 (2013).
[4] S. Muhlbauer, B. Binz, F. Jonietz, C. Pfleiderer, A. Rosch, A. Neubauer, R. Georgii, and P. Boni, Science **323**, 915 (2009).

[5] X. Z. Yu, Y. Onose, N. Kanazawa, J. H. Park, J. H. Han, Y. Matsui, N. Nagaosa, and Y. Tokura, Nature **465**, 901 (2010).
[6] S. Heinze, K. Bergmann, M. Menzel, J. Brede, A. Kubetzka, R. Wiesendanger, G. Bihlmayer, and S. Blügel, Nat. Phys. **7**, 713 (2011).
[7] J. Zang, M. Mostovoy, J. H. Han, and N. Nagaosa, Phys. Rev. Lett. **107**, 136804 (2011).
[8] S. Seki, X. Z. Yu, S. Ishiwata, and Y. Tokura, Science **336**, 198 (2012).
[9] T. Schulz, R. Ritz, A. Bauer, M. Halder, M. Wagner, C. Franz, C. Pfleiderer, K. Everschor, M. Garst, and A. Rosch, Nat. Phys. **8**, 301 (2012).
[10] X. Z. Yu, N. Kanazawa, W. Z. Zhang, T. Nagai, T. Hara, K. Kimoto, Y. Matsui, Y. Onose, and Y. Tokura, Nat. Commun. **3**, 988 (2012).
[11] J. Iwasaki, M. Mochizuki, and N. Nagaosa, Nat. Nanotech. **8**, 742 (2013).
[12] N. Romming, C. Hanneken, M. Menzel, J. E. Bickel, B. Wolter, K. Bergmann, A. Kubetzka, and R. Wiesendanger, Science **341**, 636 (2013).
[13] M. Mochizuki, X. Z. Yu, S. Seki, N. Kanazawa, W. Koshibae, J. Zang, M. Mostovoy, Y. Tokura, and N. Nagaosa, Nat. Mater. **13**, 241 (2014).
[14] A. Fert, V. Cros, and J. Sampaio, Nat. Nanotech. **8**, 152 (2013).
[15] J. Sampaio, V. Cros, S. Rohart, A. Thiaville, and A. Fert, Nat. Nanotech. **8**, 839 (2013).
[16] I. Dzyaloshinsky, Phys. Chem. Solids **4**, 241 (1958); T. Moriya, Phys. Rev. **120**, 91 (1960).
[17] V. N. Narozhnyi and V. N. Krasnorussky, J. Exp. Theor. Phys. **116**, 785 (2013).
[18] M. N. Wilson, A. B. Butenko, A. N. Bogdanov, and T. L. Monchesky, Phys. Rev. B **89**, 094411 (2014).
[19] Y. F. Li, N. Kanazawa, X. Z. Yu, A. Tsukazaki, M. Kawasaki, M. Ichikawa, X. F. Jin, F. Kagawa, and Y. Tokura, Phys. Rev. Lett. **110**, 117202 (2013); T. L. Monchesky, J. C. Loudon, M. D. Robertson, and A. N. Bogdanov, *ibid.* **112**, 059701 (2014); Y. F. Li, N. Kanazawa, X. Z. Yu, F. Kagawa, and Y. Tokura, *ibid.* **112**, 059702 (2014).
[20] X. Z. Yu, N. Kanazawa, Y. Onose, K. Kimoto, W. Z. Zhang, S. Ishiwata, Y. Matsui, and Y. Tokura, Nat. Mater. **10**, 106 (2011).
[21] F. N. Rybakov, A. B. Borisov, and A. N. Bogdanov, Phys. Rev. B **87**, 094424 (2013).
[22] R. F. Egerton, *Electron Energy-Loss Spectroscopy in the Electron Microscope* (Plenum Press, New York, 1996).
[23] K. Ishizuka and B. Allman, J. Electron Microsc. **54**, 191 (2005).
[24] S. A. Meynell, M. N. Wilson, J. C. Loudon, A. Spitzig, F. N. Rybakov, M. B. Johnson, and T. L. Monchesky, Phys. Rev. B **90**, 224419 (2014).
[25] A. Bauer and C. Pfleiderer, Phys. Rev. B **85**, 214418 (2012).
[26] A. Tonomura, X. Z. Yu, K. Yanagisawa, T. Matsuda, Y. Onose, N. Kanazawa, H. S. Park, and Y. Tokura, Nano Lett. **12**, 1673 (2012).